Augmented Reality Visualization Using Image Overlay Technology for MR-Guided Interventions

Cadaveric Bone Biopsy at 1.5 T

Jan Fritz, MD, Paweena U-Thainual, MS,†‡ Tamas Ungi, MD, PhD,§ Aaron J. Flammang, MBA, BSRT (MR),|| Edward F. McCarthy, MD,¶ Gabor Fichtinger, PhD,*†§ Iulian I. Iordachita, PhD,‡ and John A. Carrino, MD, MPH**

Purpose: The purpose of this study was to prospectively test the hypothesis that image overlay technology facilitates accurate navigation for magnetic resonance (MR)–guided osseous biopsy.

Materials and Methods: A prototype augmented reality image overlay system was used in conjunction with a clinical 1.5-T MR imaging system. Osseous biopsy of a total of 16 lesions was planned in 4 human cadavers with osseous metastases. A loadable module of 3D Slicer open-source medical image analysis and visualization software was developed and used for display of MR images, lesion identification, planning of virtual biopsy paths, and navigation of drill placement. The osseous drill biopsy was performed by maneuvering the drill along the displayed MR image containing the virtual biopsy path into the target. The drill placement and the final drill position were monitored by intermittent MR imaging. Outcome variables included successful drill placement, number of intermittent MR imaging control steps, target error, number of performed passes and tissue sampling, time requirements, and pathological analysis of the obtained osseous core specimens including adequacy of specimens, presence of tumor cells, and degree of necrosis.

Results: A total of 16 osseous lesions were sampled with percutaneous osseous drill biopsy. Eight lesions were located in the osseous pelvis (8/16, 50%) and 8 (8/16, 50%) lesions were located in the thoracic and lumbar spine. Lesion size was 2.2 cm (1.1–3.5 cm). Four (2–8) MR imaging control steps were required. MR imaging demonstrated successful drill placement inside 16 of the 16 target lesions (100%). One needle pass was sufficient for accurate targeting of all lesions. One tissue sample was obtained in 8 of the 16 lesions (50%); 2, in 6 of the16 lesions (38%); and 3, in 2 of the 16 lesions (12%). The target error was 4.3 mm (0.8–6.8 mm). Length of time required for biopsy of a single lesion was 38 minutes (20–55 minutes). Specimens of 15 of the 16 lesions (94%) were sufficient for pathological evaluation. Of those 15 diagnostic specimens, 14 (93%) contained neoplastic cells, whereas 1 (7%) specimen demonstrated bone marrow without evidence of neoplastic cells. Of those 14 diagnostic specimens, 11 (79%) were diagnostic for carcinoma or adenocarcinoma, which was concordant with the primary neoplasm, whereas, in 3 of the 14 diagnostic specimens (21%), the neoplastic cells were indeterminate.

Conclusions: Image overlay technology provided accurate navigation for the MR-guided biopsy of osseous lesions of the spine and the pelvis in human cadavers at 1.5 T. The high technical and diagnostic yield supports further evaluation with clinical trials.

Key Words: interventional MR imaging, MR-guided, MRI guidance, MRI-guided bone biopsy, osseous biopsy, augmented reality, image overlay, navigation

(*Invest Radiol* 2013;48: 00–00)

Percutaneous osseous biopsy is the preferred first-line technique for the timely and accurate diagnosis of osseous lesions and for guidance of further management.[1] Although radiologically guided osseous biopsy is frequently successfully and safely performed with fluoroscopy, sonography, and computed tomography, magnetic resonance imaging (MRI) guidance may be the technique of choice for lesions that are deeply situated, that are not visualized by other modalities, that require careful negotiation of neurovascular structures and avoidance of exposure to ionizing radiation, and that were inadequately sampled previously with other techniques.[2–9]

Despite favorable attributes of interventional MRI and reported success rates of 91% to 100%,[2–5,7,8,10] limited space and patient access inside clinical MRI systems may interfere with accurate targeting and biopsy. Augmented reality navigation can overcome this limitation by facilitating MRI guidance outside the bore of the magnet. Image overlay technology seems especially suited for osseous biopsy because it provides an augmented reality hybrid view of magnetic resonance (MR) image, target, and subject by the apparent fusion of MR images and subject.[11–16] Such a system would enable MR-guided osseous biopsy with many widely available clinical MRI systems and obviate the need for a dedicated interventional MRI system.

Therefore, the purpose of this study was to prospectively test the hypothesis that image overlay technology facilitates accurate navigation for MR-guided osseous biopsy.

MATERIALS AND METHODS

System Description

A 2-dimensional, augmented reality image overlay prototype system was used in conjunction with a clinical 1.5-T MRI system (MAGNETOM Espree; Siemens Healthcare, Erlangen, Germany)

Received for publication June 5, 2012; and accepted for publication, after revision, October 10, 2012.

From the *Russell H. Morgan Department of Radiology and Radiological Science, Johns Hopkins University School of Medicine; †Department of Mechanical Engineering and Laboratory for Computational Sensing and Robotics, The Johns Hopkins University, Baltimore, MD; ‡Department of Mechanical and Materials Engineering, §School of Computing, Queen's University, Kingston, Ontario, Canada; ||Siemens Corporate Research; Center for Applied Medical Imaging; and ¶Department of Pathology, The Johns Hopkins University School of Medicine, Baltimore, MD.

Conflicts of interest and sources of funding: Supported by grant 1 R01 CA118371-01A2 from the National Cancer Institute, Bethesda, Maryland.

P.U.T. received money for travel from Natural Sciences and Engineering Research Council of Canada.

A.J.F. has a portion of his retirement funding in Siemens stock.

I.I.I. received grant from NIH, NSF; institution has patent from Sentinelle Medical, Toronto (technology transfer for patent U.S. Provisional Application Serial No. 60/782,705 filed March 14, 2006, Publication No. WO/2007/106558, 09/20/2007; institution receives royalties from Gulmay Medical; institution received funding for research in cochlear electrode insertion from Cochlear Corporation.

J.A.C. is a board member of Vital, consultant to Quality Medical Metics and Medtronic, received money for multiple medical-legal activities; institution received grants from Siemens, Toshiba, Carestream, and Integra; author received payment for multiple grand rounds and invited lectures with honoraria; author has stock in Merge Healthcare.

Reprints: Jan Fritz, MD, The Russell H. Morgan Department of Radiology and Radiological Science, Johns Hopkins University School of Medicine, 600 N Wolfe St, Baltimore, MD 21287. E-mail: jfritz9@jhmi.edu.

ISSN: 0020-9996/13/4806–0000

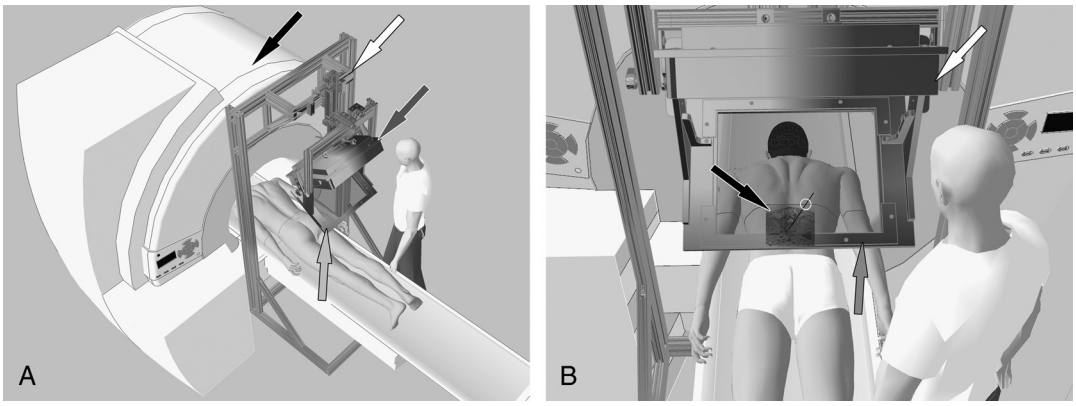

FIGURE 1. Interventional setup and image overlay system: A, Computer-aided design illustration depicts the interventional setup with a clinical, 1.5-T MRI system (black arrow) and the stand-alone augmented reality image overlay prototype system including free-standing frame (white arrow), liquid crystal display (dark-gray arrow) used for passive projection of the MR images on the semitransparent mirror (light-gray arrow), and the laser seen on the subject's skin surface. B, Computer-aided design illustration demonstrating the operator's hybrid view consisting of the projected MR image (black arrow), which apparently floats inside the subject. The line indicates a virtual needle path. The white circle marks the skin entry point, which is formed by the intersection of the laser seen in the subject's skin surface and the projected virtual biopsy path.

(Fig. 1A). The image overlay system is fully compatible with MR and permits unrestricted, diagnostic MRI without adverse effects on image quality.[17]

The system provided static MR guidance through a hybrid view created by fusion of the subject and the previously acquired corresponding MR images (Fig. 1B). The hybrid view was realized by projection and reflection of an axial MR image from a liquid crystal display to the operator via a semitransparent mirror. By moving the subject out of the bore of the magnet and under the image overlay system in the appropriate location, the projected MR image and the subject coincided. The intersection of the projected MR image and the skin surface was indicated by an axial laser plane, which was previously calibrated to the distance between the image overlay system and the isocenter of the MRI system.

A loadable module (Perkstation, https://www.assembla.com/spaces/slicerigt) for the 3D Slicer open-source medical image analysis and visualization software (version 3.6, http://www.slicer.org) was developed and used for display of the MR images, lesion identification, planning of virtual biopsy paths, and navigation of drill placement[18] (Fig. 2).

For the drill navigation, the MR image containing the virtual biopsy path with the target lesion was projected onto the subject at the appropriate location. The lesion was then targeted by maneuvering the drill along the virtual biopsy path (Fig. 2). All biopsies were performed in the axial plane.

Subjects

Four nonembalmed, full spine torso human cadavers (2 women and 2 men; age range at death, 62–78 years; mean age at death, 71 years) with osseous metastatic disease were used. One of the 4 cadavers (25%) was small in size (living body mass index [BMI], 16–18.5 kg/m^2), 2 of the 4 cadavers (50%) were medium in size (BMI, 18.5–25 kg/m^2), and 1 of the 4 cadavers (25%) were large in size (BMI, 25–30 kg/m^2).[19] The primary malignancies were pancreatic carcinoma (1/4, 25%), breast carcinoma (1/4, 25%), ovarian carcinoma (1/4, 25%), and lung cancer (1/4, 25%). All subjects were obtained and used in accordance with our institutional rules and in accordance with the Health Insurance Portability and Accountability Act. The frozen cadaveric subjects were allowed to thaw for 24 hours at room temperature (approximately 20°C–22°C) before MRI.

Research Plan

Drill biopsy of a total of 16 lesions was planned. In each subject, biopsy of 4 osseous lesions was attempted. The study was carried out on 4 different days (one subject per day) for a period of 8 weeks. The procedures were performed by an operator with 10 years of experience in percutaneous musculoskeletal procedures. Training was accomplished before the experiment with image overlay navigated osseous biopsy of 5 random osseous targets of a cadaveric specimen, which was embedded into a gel phantom.

Before each experiment, isotropic, T2-weighted MRI data sets (3-dimensional sampling perfection with application-optimized contrasts using different flip angle evolutions [SPACE] sequence; repetition time, 1000 milliseconds; echo time, 100 milliseconds; flip angle, 120 degrees; averages, 2; echo train length, 117; voxel size, 1 × 1 × 1 mm; field of view, 192 × 168 mm; base resolution, 192 pixel; phase resolution, 100%; and bandwidth, 744 Hz) of the spine and the pelvis of the respective subject were obtained.

Bone Biopsy Work Flow

Depending on the location of the target lesions and preferred access, the subject was placed prone or supine on the table of the MRI system. For all interventional MRIs, parallel imaging was used using table coil elements and a flexible loop-shaped radiofrequency surface coil (Siemens Healthcare) with a diameter of 19 cm placed over the center of the target site.

The data set used for planning and navigation consisted of an isotropic, T2-weighted MRI data set (SPACE, with the same parameters as that previously mentioned) of the region of interest, which was subsequently imported into the 3D Slicer software. The image overlay system was then calibrated for the operator by aligning his line of sight with the overlay projection using an MR-compatible, in-room keyboard in conjunction with the PerkStation module of the 3D Slicer software.

Next, the operator located the previously defined osseous lesion at the image overlay system workstation and selected an appropriate biopsy path, thereby avoiding demonstrated neurovascular structures (Figs. 2, 3, and 4). After determination of the skin entry site and the desired final position of the tip of the drill, PerkStation software module displayed the virtual biopsy path with calculated insertion depth.

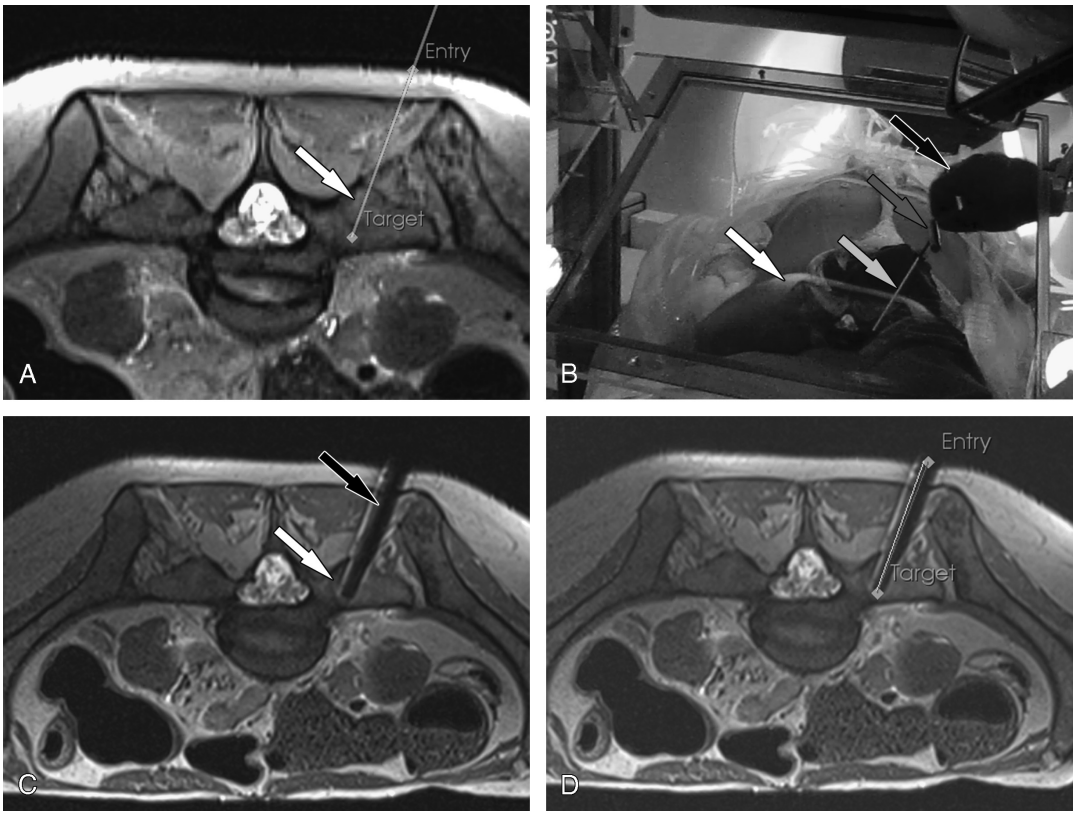

FIGURE 2. Image overlay navigated MR-guided biopsy of a right sacral osseous lesion: A, Axial T2-weighted MR image demonstrates the planned biopsy path (gray line) through an osseous lesion in the right upper sacrum (white arrow). B, Intraprocedural photograph of the operator view demonstrates the hybrid view of the subject and the projected MR image (white arrow), virtual biopsy path (light-gray arrow) through the right sacral lesion, the drill and the trocar (dark-gray arrow), and the operator's hand (black arrow). C, Axial intermediate-weighted turbo spin echo MR image after the drill placement demonstrates the drill (black arrow) through the target lesion (white arrow). D, Postprocedural assessment of the target error using the PerkStation module of the 3D Slicer software. The thick line indicates the planned biopsy path and the thin line indicates the actual biopsy path. The target error was 1.2 mm.

Then, the automatic table of the MRI system was moved to the calculated table position, which resulted in the appropriate location of the subject under the image overlay system to match the physical location with the projected MR image containing the virtual biopsy path. The operator identified the surface entry point as indicated by the virtual intersection of the laser of the overlay system and the displayed

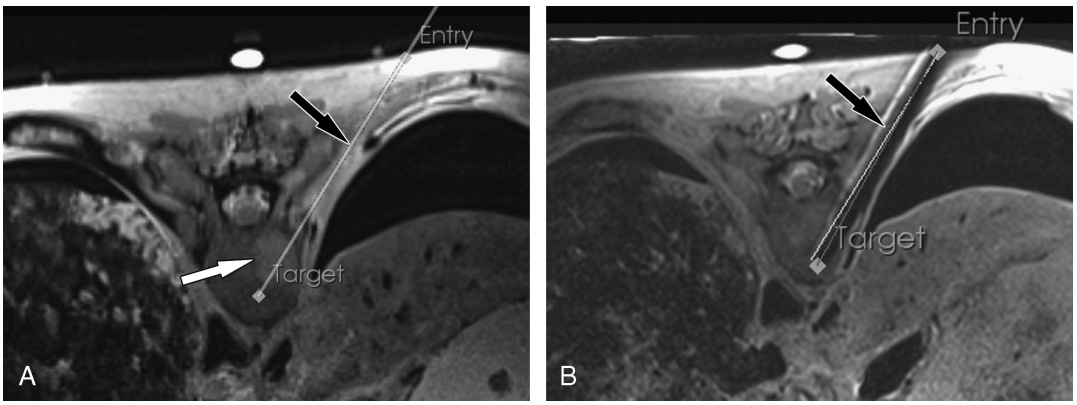

FIGURE 3. Image overlay navigated MR-guided biopsy of an osseous lesion of the eighth thoracic vertebral body: A, Axial T2-weighted MR image demonstrates the planned biopsy path (black arrow) through an osseous lesion in the eighth thoracic vertebral body (white arrow). B, Axial intermediate-weighted turbo spin echo MR image after the drill placement demonstrates the tip of the drill (black arrow) through the target lesions. Postprocedural assessment of the target error using the PerkStation module of the 3D Slicer software shows the planned biopsy path (thick line) and the actual biopsy path (thin line). The target error was 4.3 mm.

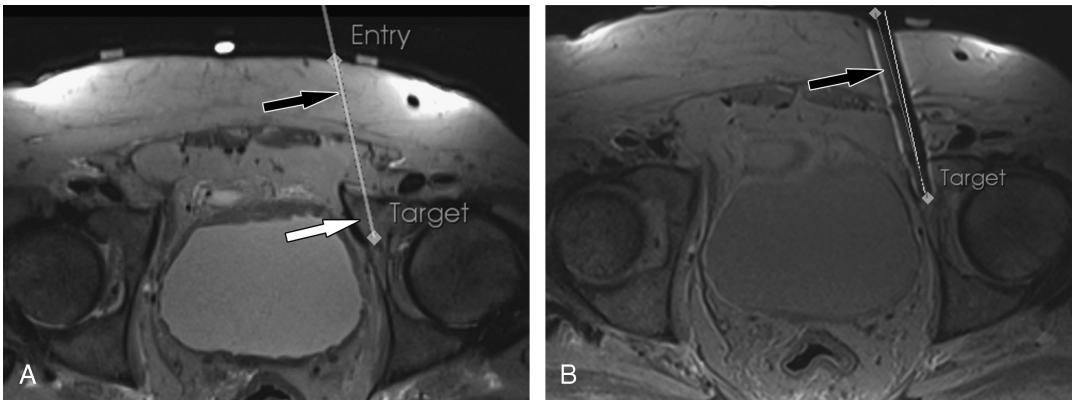

FIGURE 4. Image overlay navigated MR-guided biopsy of an osseous lesion of the left anterior acetabulum: A, Axial T2-weighted MRI demonstrates the planned biopsy path (black arrow) through an osseous lesion in the anterior aspect of the left acetabulum (white arrow). B, Axial intermediate-weighted turbo spin echo MR image after the drill placement demonstrates the tip of the drill (black arrow) through the target lesions. Postprocedural assessment of the target error using the PerkStation module of the 3D Slicer software shows the planned biopsy path (thick line) and the actual biopsy path (thin line). The target error was 3 mm.

virtual biopsy path (Figs. 1 and 2). If necessary, the surface coil was shifted to include the skin entry site centrally. The loop coil stayed in place for the entire procedure, which facilitated intermittent MRI acquisition for monitoring of the needle placement, similar to previously described techniques in patients.[4,20,21] An appropriate skin incision was created to ease the introduction of the drill system (Invivo, Orlando, FL), which consisted of a manual, 4-mm serrated hollow drill, a trocar, a stylet, and a blunt ejector.[6] The osseous drill biopsy was performed by maneuvering the drill system along the displayed virtual biopsy path into the target (Fig. 2). The stylet and the trocar were used first to penetrate the cortical bone. The trocar was subsequently advanced and locked into the penetrated cortical bone serving as an access sheath. Then, the drill was introduced into the trocar and advanced toward the lesions using its engraved depth markers and intermittent MRI (axial turbo spin echo MR sequence; repetition time/echo time, 1200/12; flip angle, 120; average, 1; echo train length, 17; slice thickness, 3 mm; number of slices, 7; field of view, 256 × 224 mm; base resolution, 320 pixels; phase resolution, 100%; bandwith, 252 Hz; and acquisition time, 22 seconds) monitoring (Fig. 2). The number of core specimens obtained depended on the operator assessment of the obtained specimen regarding its apparent adequacy for pathological analysis.

Pathological Processing

The obtained osseous core specimens were placed into a buffered formalin solution and sent for pathological analysis. The specimens subsequently underwent processing, embedding into a paraffin block, sectioning, and staining with hematoxylin and eosin. The pathological evaluation was performed by a board-certified orthopedic pathologist with 35 years of experience. The evaluation was performed blinded, without information to indicate the cadaver, primary tumor, or the anatomic location of the specimen.

Assessment of Outcome Variables

Successful drill placement was defined as MRI demonstration of the tip of the drill through the target lesion. The assessments were made qualitatively by the operator during the procedure.

The *number of intermittent MRI control steps required for appropriate drill placement* was defined as pairs of drill advancement and subsequent MRI control of the drill location.

The *target error* was defined as the Euclidean distance between the planned and final position of the tip of the drill. PerkStation was used for the calculations by comparing the planned location of the tip to the true location of the tip as manually determined on the final axial turbo spin echo MR images (Figs. 2, 3, and 4).[18] The measurements were carried out 3 times by the operator. The median mean was used.

The number of needle passes required for accurate targeting of the lesion and the number of tissue samples obtained from 1 location to obtain an appropriate amount of tissue were recorded during the individual procedures. The assessments were made qualitatively by the operator during the procedure.

The length of time for biopsy of a single lesion including planning, operator calibration, and biopsy including intermittent MRI control was recorded during the procedures.

Each specimen underwent pathological evaluation including determination of the technical adequacy of the submitted specimens for histopathological diagnosis, presence of tumor cells, ratio of necrotic to viable tumor cells, and type of neoplastic cells.

Statistical and Quantitative Assessments

Statistical analysis was performed with statistical software (JMP, version 7.01; SAS Institute Inc, Cary, NC). Categorical variables were expressed as frequencies and proportions. Quantitative variables were expressed as the median with minimum and maximum values. Intrarater variability was expressed by use of the coefficient of variation (CV) as $CV = \sigma/\mu$, wherein σ is the first standard deviation and μ is the arithmetic mean. A $P < 0.05$ was considered to indicate a significant difference.

RESULTS

A total of 16 osseous lesions were sampled with percutaneous osseous drill biopsy. Eight lesions were located in the osseous pelvis (8/16, 50%) and 8 (8/16, 50%) lesions were located in the thoracic and lumbar spine. Of the spinal lesions, 5 of the 8 biopsy paths (62%) were parapedicular and 3 of the 8 biopsy paths (38%) were transpedicular. Ten of the 16 lesions (62%) were located on the subject's right body half and 6 of the 16 lesions (38%) were located on the subject's left body half. The procedures were feasible in all 3 sizes of the cadavers. For the large cadaver, the height of the individually adjustable reflective mirror of the image overlay system was increased. The average largest diameter of a lesion was 2.2 cm (range, 1.1–3.5 cm). The average distance between the skin surface and the lesions was 5.1 cm (3.5–7.8 cm) for

TABLE 1. Results of Pathological Evaluation

Demographics			Results of Pathological Evaluation			
Cadaver Number	**Primary Neoplasm**	**Lesion Number**	**Adequacy of Specimens**	**Neoplastic Cells**	**Degree of Necrosis**	**Type of Neoplasm**
1	Breast carcinoma	1	Diagnostic	Present	80%	Adenocarcinoma
		2	Diagnostic	Present	80%	Adenocarcinoma
		3	Diagnostic	Present	50%	Adenocarcinoma
		4	Diagnostic	None	—	—
2	Non–small cell lung cancer	1	Diagnostic	Present	50%	Carcinoma
		2	Diagnostic	Present	50%	Carcinoma
		3	Diagnostic	Present	100%	Indeterminate
		4	Nondiagnostic	—	—	—
3	Pancreatic adenocarcinoma	1	Diagnostic	Present	100%	Carcinoma
		2	Diagnostic	Present	100%	Carcinoma
		3	Diagnostic	Present	100%	Carcinoma
		4	Diagnostic	Present	100%	Indeterminate
4	Ovarian adenocarcinoma	1	Diagnostic	Present	90%	Carcinoma
		2	Diagnostic	Present	100%	Carcinoma
		3	Diagnostic	Present	100%	Carcinoma
		4	Diagnostic	Present	100%	Indeterminate

the pelvic lesions and 6.8 cm (4.1–9.1 cm) for the lesions located in the spine. An average of 4 (2–8) steps of MRI control was required to navigate the drill into the target lesion. Successful placement of the drill inside the lesion was demonstrated in 16 of the 16 lesions (100%) by MRI. Each lesion (16/16, 100%) was successfully targeted with 1 needle pass. To obtain a sufficient amount of tissue from the same location, 1 tissue sample was required in 8 of the 16 lesions (50%), 2 tissue samples were required in 6 of the 16 lesions (38%), and 3 tissue samples were required in 2 of the 16 lesions (12%). The target error was 4.3 ± 1.2 mm (range, 0.8–6.8 mm) (CV, 7.2% ± 5.9%; range, 7.7%7–12.8%). The average length of time required for biopsy of a single lesion was 38 minutes (20–55 minutes).

The results of the pathological analysis are detailed in Table 1. The specimens of 15 of the 16 lesions (94%) were sufficient for pathological analysis and diagnosis, whereas the specimen of 1 of the 16 lesions (6%) was nondiagnostic. Of those 15 diagnostic specimens, 14 (93%) were diagnosed with neoplastic cells, whereas 1 specimen (7%) demonstrated bone marrow without evidence of neoplastic cells. Of those 14 diagnostic specimens, 11 specimens (79%) were diagnostic for either carcinoma or adenocarcinoma, which was concordant with the primary neoplasm, whereas, in 3 of the 14 diagnostic specimens (21%), the neoplastic cells were indeterminate.

DISCUSSION

The results of our study show that image overlay technology provided accurate navigation for MR-guided osseous biopsy of the spine and the pelvis of human cadavers. The average target error was 4.3 mm. The obtained specimens were technically adequate for pathological analysis in 94% (15/16) of the biopsied lesions. The neoplastic cells were diagnosed in 93% of the analyzed specimens. Seventy-nine percent were diagnostic for carcinoma or adenocarcinoma, which was concordant with the primary neoplasm.

The usefulness of MR-guided biopsy in a carefully selected subset of patients has been demonstrated by multiple investigators.[2–5,7–10,22–25] Indications include osseous lesions that are not adequately visualized by other modalities, avoidance of exposure to ionizing radiation, and lesions that were previously sampled inadequately with other techniques. MR–guided biopsy of osseous lesions in children and adolescents exemplarily complies with as low as reasonably achievable (ALARA) practice mandate.[4,5] The diagnostic accuracy of MR-guided biopsy of osseous lesions ranges between 91% to 100%.[3,7,8,10,14] Manual or piezoelectric power drill system may be used.[6] Contrast-enhanced MR-guided osseous biopsy enables selective targeting and biopsy of viable areas inside osseous lesions and may therefore increase the diagnostic accuracy.[10]

In comparison with 0.2- to 0.5-T MRI systems, MR-guided osseous biopsy at 1.5-T field-strength magnets results in substantially higher signal-to-noise ratios, the use of higher bandwidths, and increased chemical shift. The higher MR signal may be used for improved spatial, temporal, contrast resolution, or combinations thereof. The higher bandwidths can be used to optimize the passively created drill artifact and minimize potential overestimations of size. Increased chemical shift enables the use of spectral fat saturation techniques, which may be helpful in increasing lesion conspicuity.

MR–guided osseous biopsy using a combination of closed-bore 1.5-T MRI systems and c-arm fluoroscopy has been shown to be feasible[26,27]; however, it was not widely adopted because of limited space inside the bore of the magnet. More recently introduced clinical wide-bore MRI systems minimize the risk for contact of the biopsy system with the housing of the bore and allow device placement inside the bore.[20] Although needle puncture can be accurately performed inside the bore,[28–30] the distance to the isocenter may hamper accurate placement and advancement of a drill system inside the bore. Instead, drill advancement may be performed outside the bore with indirect navigation by a separate in-room monitor.[14] The resulting visual and spatial separation of MR image, biopsy path, and target requires mental transfer of the image information onto the patient and possibly introduces inaccuracy. Image overlay navigation, on the other hand, realizes simultaneous visualization of the MR images and the target. The combination of MR image and target results in an intuitive hand-eye coordination, which is similar to a surgical procedure. However, it may be emphasized that, although image overlay navigation supports the mental transfer of data and device actions, essential interventional skills, such as translation of image information into an appropriate and safe needle path, and sufficient practical experience in navigation and placement of drill devices remain a prerequisite.

The target error of 4.3 mm in our study was sufficient for accurate biopsy of all osseous targets and avoidance of vulnerable, nontargeted structures. This target error, in part, relates to the large

size of the trocar (6-mm outer diameter), the size of the hollow drill itself (4-mminner diameter), and the deeply situated osseous lesions, which required a longer intraosseous course of the drill. Comparison with reported target errors of other navigation systems for MR-guided interventions is limited by the use of different targets (eg, more superficially located soft tissue targets), the use of injection needles (eg, 20-G spinal needles), and differences in the methods of error calculations but range between 1.1 to 7.5 mm.[31–36]

Image overlay navigation has the potential to simplify the work flow of MR-guided osseous biopsy at higher field strength, to obviate the requirement for a dedicated interventional MRI system, and to overcome the limited access inside the bore of a magnet.[25] Because drill advancement is performed outside the bore, image overlay technology can be used with almost any MRI system with a horizontal bore configuration and a moveable patient table.

The 19-cm width of the loop coil provides sufficient space for skin preparation and surgical draping and can therefore be kept in place during the entire procedure.[4,20] The use of a fenestrated drape with adhesive margins covers the coil and creates an isolated sterile field. With this technique, the surface coil does not interfere with sterility or device placement.

Our study had limitations. First, because of the use of cadavers, effects of patient motion and respiration were not present, which may influence the performance of static image overlay navigation. Second, because the location of osseous lesions was unknown, the MRI data set, which was later used for planning, covered the entire thoracolumbar spine and the pelvis to identify the osseous lesions. Therefore, the acquisition time of the planning MRI data set of each individual lesion was not available and therefore not included in the length of time required for biopsy of a single lesion. As a reference, the acquisition time for the planning volume covering 1 lumbar vertebral body is approximately 3 minutes. Third, although efforts were made to use a high number of cadavers, 4 osseous biopsies were performed in each of the 4 cadavers, which may have resulted in clustering of data. Fourth, osseous metastases were selected on the basis of MRI evaluation. Because of the lack of intentionally obtained true negative biopsy specimens and the lack of gross pathological correlation of the biopsied osseous in situ lesions, diffuse neoplastic bone marrow infiltration could not be excluded. However, because of the similarity of our results across the 4 cadavers, this scenario seems unlikely. Fifth, because of the overall high degree of necrosis of neoplastic cell, the pathological determination of the primary tumor was somewhat limited. Although this may be related to the preservation process of the cadavers, the differentiation of benign from malignant is generally more often achieved than an exact diagnosis of the neoplastic cells.[37,38]

A restriction of the current image overlay system is the limitation of the needle path to the axial image plane, which presently prevents the use of the powerful multiplanar capabilities of interventional MRI. Although the axial image plane was sufficient for successful sampling of the targets in this study, nonaxial needle paths are required for targeting lesions in a challenging anatomic location, in which crucial soft tissue structures such as nerves, vessel, and parenchymal organs prevent an axial needle path. Future extensions of this image overlay system include the implementation of such nonaxial image navigation capabilities. This could be realized by the addition of an axial tilting mechanism of the semitransparent mirror or rotation of the semitransparent monitor into the sagittal image plane.

In summary, image overlay technology provided accurate navigation for MR-guided biopsy of osseous lesions of the spine and the pelvis in human cadavers at 1.5 T with a high technical and diagnostic yield. It has the potential to simplify the work flow of MR-guided osseous biopsy and overcome spatial limitation of clinical MRI systems. It can be used with most MRI systems with a horizontal bore configuration and a moveable patient table and potentially increases the number of sites capable of MR-guided osseous biopsy. The high technical and diagnostic yield of MR-guided osseous biopsy in our study supports further evaluation with clinical trials.

REFERENCES

1. Jelinek JS, Murphey MD, Welker JA, et al. Diagnosis of primary bone tumors with image-guided percutaneous biopsy: experience with 110 tumors. *Radiology*. 2002;223:731–737.
2. Carrino JA, Blanco R. Magnetic resonance–guided musculoskeletal interventional radiology. *Semin Musculoskelet Radiol*. 2006;10:159–174.
3. Smith KA, Carrino J. MRI-guided interventions of the musculoskeletal system. *J Magn Reson Imaging*. 2008;27:339–346.
4. Fritz J, Tzaribachev N, Thomas C, et al. Magnetic resonance imaging–guided osseous biopsy in children with chronic recurrent multifocal osteomyelitis. *Cardiovasc Intervent Radiol*. 2012;35:146–153.
5. Koenig CW, Duda SH, Truebenbach J, et al. MR-guided biopsy of musculoskeletal lesions in a low-field system. *J Magn Reson Imaging*. 2001;13:761–768.
6. Konig CW, Trubenbach J, Bohm P, et al. Magnetic resonance–guided transcortical biopsy of bone marrow lesions using a magnetic resonance imaging–compatible piezoelectric power drill: preliminary experience. *Invest Radiol*. 2003;38:159–163.
7. Carrino JA, Khurana B, Ready JE, et al. Magnetic resonance imaging–guided percutaneous biopsy of musculoskeletal lesions. *J Bone Joint Surg Am*. 2007;89:2179–2187.
8. Blanco SR, Klemola R, Ojala R, et al. MRI-guided trephine biopsy and fine-needle aspiration in the diagnosis of bone lesions in low-field (0.23 T) MRI system using optical instrument tracking. *Eur Radiol*. 2002;12:830–835.
9. Ojala R, Sequeiros RB, Klemola R, et al. MR-guided bone biopsy: preliminary report of a new guiding method. *J Magn Reson Imaging*. 2002;15:82–86.
10. Parkkola RK, Mattila KT, Heikkila JT, et al. Dynamic contrast-enhanced MR imaging and MR-guided bone biopsy on a 0.23 T open imager. *Skeletal Radiol*. 2001;30:620–624.
11. Fichtinger G, Deguet A, Masamune K, et al. Image overlay guidance for needle insertion in CT scanner. *IEEE Trans Biomed Eng*. 2005;52:1415–1424.
12. Fischer GS, Deguet A, Schlattman D, et al. MRI image overlay: applications to arthrography needle insertion. *Stud Health Technol Inform*. 2006;119:150–155.
13. Weiss CR, Marker DR, Fischer GS, et al. Augmented reality visualization using image-overlay for MR-guided interventions: system description, feasibility, and initial evaluation in a spine phantom. *AJR Am J Roentgenol*. 2011;196:W305–W307.
14. Fritz J, Thainual P, Ungi T, et al. Augmented reality visualization with image overlay for MRI-guided intervention: accuracy for lumbar spinal procedures with a 1.5-T MRI system. *AJR Am J Roentgenol*. 2012;198:W266–W273.
15. Fritz J, U-Thainual P, Ungi T, et al. Augmented reality visualisation using an image overlay system for MR-guided interventions: technical performance of spine injection procedures in human cadavers at 1.5 Tesla. *Eur Radiol*. 2013;23(1):235–245.
16. Fritz J, Thainual P, Ungi T, et al. Augmented reality visualization with use of image overlay technology for MR imaging–guided interventions: assessment of performance in cadaveric shoulder and hip arthrography at 1.5 T. *Radiology*. 2012;265:254–259.
17. U-Thainual P, Fritz J, Moonjaita C, et al. MR image overlay guidance: system evaluation for preclinical use. *Int J Comput Assist Radiol Surg*. 2012 Aug 25. [Epub ahead of print].
18. Vikal S, Thainual P, Carrino JA, et al. Perk Station—percutaneous surgery training and performance measurement platform. *Comput Med Imaging Graph*. 2010;34:19–32.
19. World Health Organization. Obesity: preventing and managing the global epidemic. Report of a WHO consultation. *World Health Organ Tech Rep Ser*. 2000;894:i–253. http://www.who.int/nutrition/publications/obesity/WHO_TRS_894/en/.
20. Fritz J, Henes JC, Thomas C, et al. Diagnostic and interventional MRI of the sacroiliac joints using a 1.5-T open-bore magnet: a one-stop-shopping approach. *AJR Am J Roentgenol*. 2008;191:1717–1724.
21. Streitparth F, Walter T, Wonneberger U, et al. Image-guided spinal injection procedures in open high-field MRI with vertical field orientation: feasibility and technical features. *Eur Radiol*. 2010;20:395–403.
22. Blanco SR, Carrino JA. Musculoskeletal interventional MR imaging. *Magn Reson Imaging Clin N Am*. 2005;13:519–532.
23. Genant JW, Vandevenne JE, Bergman AG, et al. Interventional musculoskeletal procedures performed by using MR imaging guidance with a vertically open MR unit: assessment of techniques and applicability. *Radiology*. 2002;223:127–136.
24. Lewin JS, Petersilge CA, Hatem SF, et al. Interactive MR imaging–guided biopsy and aspiration with a modified clinical C-arm system. *AJR Am J Roentgenol*. 1998;170:1593–1601.

25. Weiss CR, Nour SG, Lewin JS. MR-guided biopsy: a review of current techniques and applications. *J Magn Reson Imaging*. 2008;27:311–325.
26. Adam G, Neuerburg J, Bucker A, et al. Interventional magnetic resonance: initial clinical experience with a 1.5-tesla magnetic resonance system combined with c-arm fluoroscopy. *Invest Radiol*. 1997;32:191–197.
27. Neuerburg JM, Adam G, Buecker A, et al. MRI-guided biopsy of bone in a hybrid system. *J Magn Reson Imaging*. 1998;8:85–90.
28. Fritz J, Thomas C, Tzaribachev N, et al. MRI-guided injection procedures of the temporomandibular joints in children and adults: technique, accuracy, and safety. *AJR Am J Roentgenol*. 2009;193:1148–1154.
29. Fritz J, Thomas C, Clasen S, et al. Freehand real-time MRI-guided lumbar spinal injection procedures at 1.5 T: feasibility, accuracy, and safety. *AJR Am J Roentgenol*. 2009;192:W161–W167.
30. Fritz J, Tzaribachev N, Thomas C, et al. Evaluation of MR imaging guided steroid injection of the sacroiliac joints for the treatment of children with refractory enthesitis-related arthritis. *Eur Radiol*. 2011;21:1050–1057.
31. Busse H, Garnov N, Thormer G, et al. Flexible add-on solution for MR image–guided interventions in a closed-bore scanner environment. *Magn Reson Med*. 2010;64:922–928.
32. Christoforou E, Akbudak E, Ozcan A, et al. Performance of interventions with manipulator-driven real-time MR guidance: implementation and initial in vitro tests. *Magn Reson Imaging*. 2007;25:69–77.
33. Hata N, Tokuda J, Hurwitz S, et al. MRI-compatible manipulator with remote-center-of-motion control. *J Magn Reson Imaging*. 2008;27:1130–1138.
34. Silverman SG, Collick BD, Figueira MR, et al. Interactive MR-guided biopsy in an open-configuration MR imaging system. *Radiology*. 1995;197:175–181.
35. Tokuda J, Fischer GS, Csoma C, et al. Software strategy for robotic transperineal prostate therapy in closed-bore MRI. *Med Image Comput Comput Assist Interv*. 2008;11(pt 2):701–709.
36. Wacker FK, Vogt S, Khamene A, et al. An augmented reality system for MR image–guided needle biopsy: initial results in a swine model. *Radiology*. 2006;238:497–504.
37. Gogna A, Peh WC, Munk PL. Image-guided musculoskeletal biopsy. *Radiol Clin North Am*. 2008;46:455–473.
38. Welker JA, Henshaw RM, Jelinek J, et al. The percutaneous needle biopsy is safe and recommended in the diagnosis of musculoskeletal masses. *Cancer*. 2000;89:2677–2686.